

Report of Visiting Scientist mission NWP_VS12_03

Document NWPSAF-MO-VS-048



Version 1.0

27 May 2013

Evaluation of control variables for the assimilation of cloud-affected infrared radiances

Pauline Martinet^a, William Bell^b, Ed Pavelin^b and John Eyre^b

^a Météo France, Toulouse, France; ^b Met Office, Exeter, UK

 	Evaluation of control variables for the assimilation of cloud-affected infrared radiances	Doc ID : NWPSAF-MO-VS-048 Version : 1.0 Date : 27 May 2013
---	---	--

Evaluation of control variables for the assimilation of cloud-affected infrared radiances

Pauline Martinet^a, William Bell^b, Ed Pavelin^b and John Eyre^b

^a Météo France, Toulouse, France; ^b Met Office, Exeter, UK

This documentation was developed within the context of the EUMETSAT Satellite Application Facility on Numerical Weather Prediction (NWP SAF), under the Cooperation Agreement dated 29 June 2011, between EUMETSAT and the Met Office, UK, by one or more partners within the NWP SAF. The partners in the NWP SAF are the Met Office, ECMWF, KNMI and Météo France.

Copyright 2013, EUMETSAT, All Rights Reserved.

Evaluation of control variables for the assimilation of cloud-affected infrared radiances.

Pauline Martinet^a, William Bell^b, Ed Pavelin^b, John Eyre^b

^a Météo France, Toulouse, France

^b Met Office, Exeter, UK

May 27, 2013

Abstract

This paper describes some preliminary investigations of assimilating cloud-affected infrared radiances with the use of cloud fraction as a new control variable. The advanced radiative transfer model RTTOV-CLD is used to simulate IASI spectra directly from a short range forecast field including liquid water content, ice water content and cloud fraction profiles. This approach enables a more realistic representation of clouds and is able to deal with multi-layer clouds by taking into account cloud scattering. The approach is illustrated with 1D-Var retrievals in the context of observing system simulation experiments. The results are promising and encouraging with the 1D-Var being able to decrease or increase the cloud amounts to reduce the observation minus background departures.

1 Introduction

All numerical weather prediction (NWP) centres intend to increase the number of satellite observations assimilated in cloudy conditions. Indeed, with about 80 % of satellite data at least partially covered by clouds, the assimilation of infrared (IR) radiances is very restrictive if only clear scenes are assimilated. This under-exploitation of IR satellite data, mainly caused by aggressive thinning, is also explained by the rejection of cloud-affected radiances during the assimilation process because of large innovations (observation minus background) due to cloud mislocation or deficiencies in the modelling of clouds, either in radiative transfer (RT) models or NWP models. However, the high correlation between cloud cover and meteorologically sensitive areas underlines the need to use infrared observations in presence of clouds (McNally (2002), Fourrié and Rabier (2004)). The all-sky approach used at the European Centre for Medium Range Weather Forecasts (ECMWF) for the assimilation of microwave data (Geer et al (2008), Bauer et al (2010), Geer et al (2010)) was a significant advance towards the assimilation of cloud and precipitation affected radiances. However, in the IR, an incorrect modelling of clouds leads to increased errors in the radiative transfer (RT) calculations which is very sensitive to cloud microphysical properties, making the assimilation of cloud-affected infrared radiances more difficult.

Despite the difficulty in assimilating IR satellite data in cloudy conditions, most NWP centres have progressed in the use of these data. All the existing approaches use a simplified modelling of clouds which are assumed to be represented by single layers of opaque clouds with a cloud emissivity equal to one. Clouds are characterized by a cloud top pressure (CTOP) and an effective cloud fraction (Ne) (Pavelin et al. (2008), Pangaud et al. (2009), McNally (2009), Guidard et al. (2011), Lavanant et al. (2011)). However, with most of these techniques, too few data are assimilated due to the restriction to opaque scenes and channels with weak cloud sensitivity.

The aim of this work was to explore new assimilation techniques based on an explicit analysis of microphysical

variables (liquid water content, ice water content and cloud fraction) for the simulation and the assimilation of cloud-affected IR radiances. New convective scale models (such as the Météo France AROME and Met Office UKV models) produce forecasts of cloud variables with a high resolution. These profiles can be used in the advanced radiative transfer model RTTOV-CLD (Hocking et al. (2010)) to simulate cloudy IASI spectra taking into account multi-layer and mixed-phase clouds but also cloud scattering. The study of Martinet et al (2013,a) with the AROME model has already shown encouraging results for the inclusion of liquid water content and ice water content in the control vector of the NWP SAF Met Office 1D-Var code (Pavelin and Collard (2009)).

This study follows this work by exploring the possibility of adding the cloud fraction as an additional state vector variable with liquid water content and ice water content. The inclusion of the cloud fraction (cfrac) is important as the RT model RTTOV-CLD is highly sensitive to the cloud fraction and to obtain a cloud fraction profile consistent with the analyzed liquid water content (lwc) and ice water content (iwc) profiles. It has been decided to add the cloud fraction in the control vector of the 1D-Var instead of using a diagnostic relationship to derive the cloud fraction from the analyzed cloud variables. In fact, the use of a diagnostic relationship would couple the cloud fraction and the hydrometeors strongly with a formulation from the numerical weather prediction model that is certainly not appropriate to fit IASI observations. Thus, we carried out one-dimensional variational (1D-Var) retrievals of cloud variables (lwc, iwc, cloud fraction) with an extended version of the NWP SAF 1D-Var code. To evaluate the cloudy retrievals, synthetic IASI observations were used in the manner of Observing System Simulation Experiments (OSSE). Cloudy profiles from the French convective scale model AROME were used to simulate the IASI observations.

Three cloudy profiles representative of semi-transparent cloud, high opaque cloud and low opaque cloud were used to investigate three main questions:

- Are we able to properly modify the cloud variables of an already existing cloud layer ?
- Are we able to properly create new cloudy layers in clear atmospheric layers in the background ?
- Can we generalize these results on a global dataset of cloudy profiles ?

In section 2, the NWP SAF 1D-Var code is presented as well as the background error covariance matrix used for this study. Section 3 presents 1D-Var retrievals of three atmospheric profiles where the clouds have been modified in cloudy layers already existing in the background. Section 4 presents some 1D-Var retrievals for which the cloud has to be moved in atmospheric layers not covered by clouds in the background. In these two sections, the 1D-Var retrievals have been carried out on three atmospheric profiles: a high opaque cloud, a low liquid cloud and a semi-transparent ice cloud. Section (5) generalizes the results of the previous sections by performing 1D-Var retrievals on a large sample of atmospheric profiles. The root-mean-square errors of the analysis and the background against the ‘truth’ are compared. This paper concludes with a summary of the main findings and future prospects.

2 Experimental framework

2.1 1D-Var framework

The 1D-Var analysis described here is based on linear optimal estimation but some non-linearities are taken into account through the update of the Jacobians at each iteration. The best approximation of the atmospheric state \mathbf{x} is a combination of a vector of observations \mathbf{y} and a background state \mathbf{x}_b from a short-range forecast. The observations are linked to the atmospheric state by an observation operator H including interpolations from the observation space to the model space and a radiative transfer model. The best linear unbiased estimation of the atmospheric state is obtained by minimizing the cost function:

$$J(\mathbf{x}) = \frac{1}{2}(\mathbf{x} - \mathbf{x}_b)^T \mathbf{B}^{-1}(\mathbf{x} - \mathbf{x}_b) + \frac{1}{2}(\mathbf{y} - \mathbf{H}(\mathbf{x}))^T \mathbf{R}^{-1}(\mathbf{y} - \mathbf{H}(\mathbf{x})) \quad (2.1)$$

where \mathbf{R} is the measurement error covariance matrix, \mathbf{B} is the background-error covariance matrix, T is the transpose operator and $^{-1}$ the inverse operator. During the minimization process, a Levenberg-Marquardt descent algorithm is applied.

2.2 Cloudy background error covariance matrix

To optimize the assimilation of cloudy observations, appropriate background error covariances that include couplings with the other model variables should be considered. The computation of cloudy \mathbf{B} matrices is still an active area of research but a cloudy \mathbf{B} matrix for temperature, humidity, liquid water content and ice water content was previously computed and tested for the AROME model (Martinet et al (2013,a)).

For that purpose, background-error covariances have been diagnosed for cloudy areas with a method similar to the one described by Montmerle and Berre (2010) to diagnose forecast errors in precipitating areas. The background-error statistics were derived from an AROME ensemble assimilation, that considers explicit observation perturbations and implicit background perturbations through the cycling, coupled with the operational ensemble assimilation at global scale AEARP (Desroziers et al. (2008)). They were calculated from a set of 18 convective cases observed during the months of July, August and September 2009. For separating cloudy and clear areas, a geographical cloud mask has been applied to the forecast differences $\epsilon_b^{kl} = \mathbf{x}_b^k - \mathbf{x}_b^l$ between members (k, l) . For each member, only profiles whose vertically integrated cloud contents exceed 0.01 g.kg^{-1} have been taken into account to perform the statistics. A similar approach to Michel et al. (2011), which uses an extension of the multivariate formalism proposed by Berre (2000), has been chosen for the forecast errors of q_l and q_i , allowing couplings with errors of temperature and of unbalanced specific humidity, the temperature being univariate.

This cloudy \mathbf{B} matrix was not available for the cloud fraction. It was decided to use our AROME profile dataset to compute the standard deviation of the cloud fraction for each atmospheric level. These standard deviation values were used as the diagonal elements of the cloud fraction background error. The dataset used for the computation of the standard deviation contains both high clouds and low clouds without any distinction between semi-transparent and opaque clouds. The aim was to obtain a static matrix that can be used for most cloudy cases. We also decided to add a small correlation of 0.1 between the cloud fraction and the liquid water content and the ice water content. To have some consistency between the increments in adjacent levels, vertical correlations that follow a Gaussian distribution were added. The number of adjacent levels that are correlated between each other was decided after testing different \mathbf{B} matrices. The value of 12 vertical levels correlated was found to be the best for the retrieval of the different cloud variable: lwc, iwc, cfrac. Figure 1 shows the entire \mathbf{B} matrix with the different block of covariances. The variables in the state vector are composed of 60 levels and are sorted in this order: temperature, humidity, liquid water content, ice water content and cloud fraction. The standard deviation of background errors for each cloud variable is presented in figure 2.

3 Modification of cloudy layers already existing in the background

Our first study was to evaluate the feasibility of modifying at the same time the three cloud variables (lwc, iwc, cloud fraction) in cloudy layers already existing in the background. This study was necessary to give preliminary answers about the relevance of the inclusion of the cloud fraction in the state vector.

3-hour forecasts from the convective scale model AROME are used to provide the ‘truth’ (\mathbf{x}_t) used as the reference. These true profiles are perturbed to provide the background profile used in the 1D-Var and the IASI observation \mathbf{y} :

$$\mathbf{y} = \mathbf{H}(\mathbf{x}_t) + \epsilon_o \mathbf{R}^{\frac{1}{2}} \quad (3.1)$$

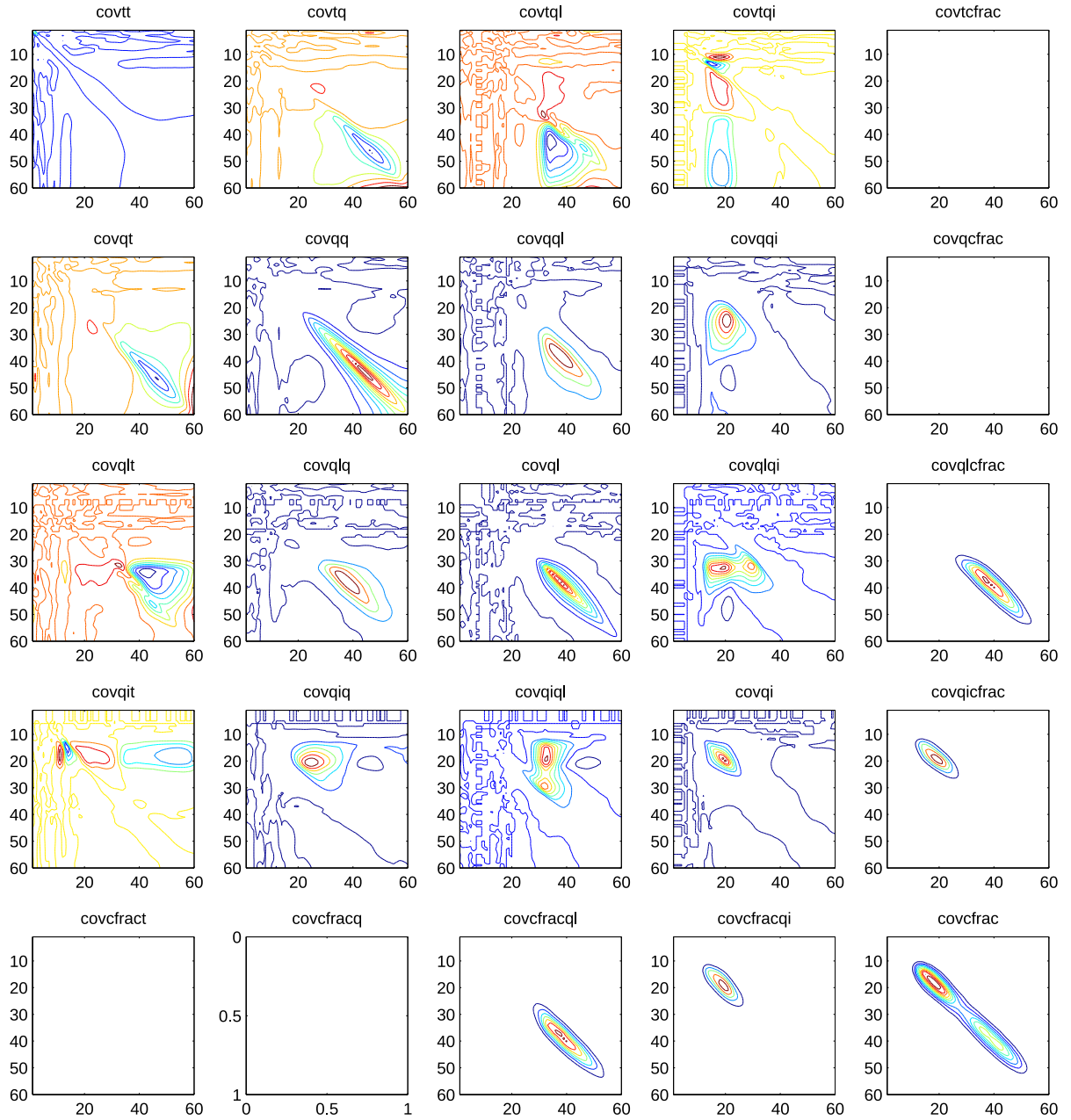


Figure 1: Cloudy background error covariance matrix used in the 1D-Var. The state vector contains the 60 vertical levels of each variable in the following order: temperature (t), humidity (q), liquid water content (ql), ice water content (qi) and cloud fraction (frac).

where \mathbf{y} is the perturbed observation, \mathbf{R} is the observation error covariance matrix, $H(\mathbf{x}_t)$ is the observation simulated from the ‘true’ profile, and ϵ_o is a random vector drawn from a Gaussian distribution with zero mean and unit standard deviation. The \mathbf{R} matrix is assumed diagonal with values constructed from the instrumental noise provided by CNES. A constant error is also added to take into account the radiative transfer model error (0.2 K for liquid cloud and 0.5 K for ice cloud).

The 1D-Var retrievals have been performed with a subset of 480 IASI channels. This subset is composed of the first 346 IASI channels of the operational channel subset used at ECMWF (Collard and McNally (2009)). These channels were chosen for their properties in clear conditions. A subset of 134 new channels were added for their sensitivity to cloud variables (Martinet et al (2013,b)).

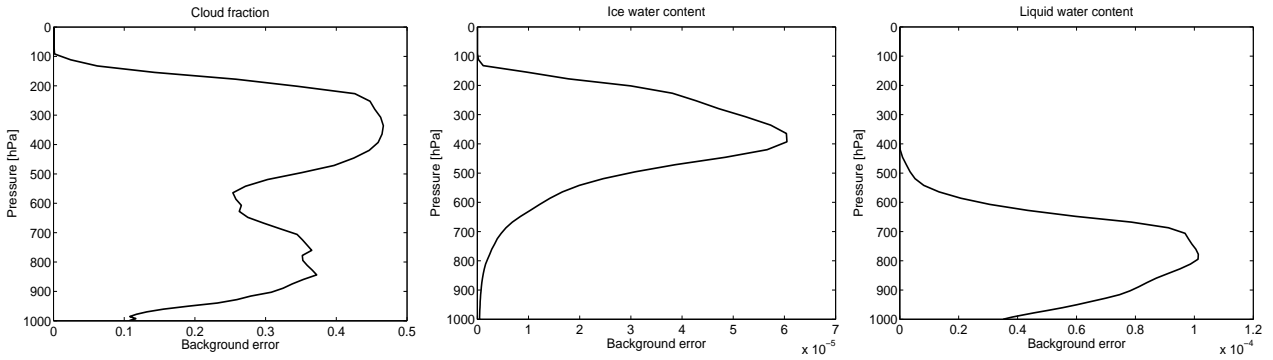


Figure 2: Background error for cloud fraction (left panel), ice water content (middle panel) and liquid water content (right panel)

We studied three cloudy profiles: one low liquid cloud, one semi-transparent ice cloud and one opaque ice cloud. For each cloudy profile, the ‘true’ AROME profiles are perturbed to increase the cloud fraction by 0.1 and the humidity and the cloud variables by 10 % in the background profile. The observation minus background departures are thus positive meaning an excessive cloud amount in the background compared to the observation.

3.1 1D-Var retrievals

The first example is a low liquid cloud shown in figure 3. In this figure, observation minus background (O-B) and observation minus analysis (O-A) departures, profiles of background, true and analysis of humidity, cloud water contents and cloud fraction are shown. The O-B departures are decreased as expected by the 1D-Var in window channels sensitive to clouds. In order to remove the excess cloud, the 1D-Var decreases the liquid water content but the increment is slightly too big. However, the cloud fraction is decreased from 1 to 0.9 in the highest cloudy layer in good agreement with the ‘true’ profile. Some non zero values appear above and below the cloud after the analysis due to the vertical correlations used in the static cloudy **B** matrix. This spread of low clouds under an inversion layer can be problematic in an operational context. The use of a state-dependent **B** matrix would help to stop the spreading of the cloudy layer. We can also think about penalizing the cost function when clouds are created in a dry atmospheric layer but this study was beyond the scope of the mission.

The second example is an opaque cloud with mixed-phase layers containing both liquid water and ice (figure 4). Large O-B departures are observed with values up to 8 K for longwave window channels and 15 K for shortwave window channels. These values are successfully decreased by the analysis with O-A departures much closer to zero. The ice water content profile is also effectively decreased to fit the ‘true’ profile. The cloud fraction analysis is also better than the background for both cloudy layers. However, the cloud fraction analysis fits better the ‘true’ profile in the highest cloudy layer (200-450 hPa) than the lowest layer. The modification of the cloud fraction associated to the liquid cloud layer located under 800 hPa is due to some transparency of the cloud. Even if this cloud was classified as opaque because of an effective cloud fraction value above 0.9, the cloud is not dense enough (10^{-5}kg.kg^{-1}) to avoid the contamination by low levels. This is illustrated by the cloud fraction Jacobians in figure 5 after multiplying the ice water content profile by 10. We can notice that the Jacobians calculated with the initial cloud fraction profile (left panel) have significant values around 900 hPa corresponding to the liquid cloud layer under the ice cloud layer. If we multiply the ice water content profile by 10 (right panel) making the cloud more opaque (10^{-4}kg.kg^{-1} instead of 10^{-5}kg.kg^{-1}), this sensitivity to low levels disappear.

The third example is a semi-transparent ice cloud (figure 6). Large O-B departures are observed with val-

ues up to 7 K for longwave window channels. The minimization seems to work well with O-A departures much smaller than the O-B departures. The ice water content profile is decreased effectively at the cloud top (200 hPa) but the increment is slightly too big at 250 hPa. In order to remove the excess cloud, the cloud fraction is well reduced by the 1D-Var even if the increment should be bigger for a better fit of the ‘true’ profile.

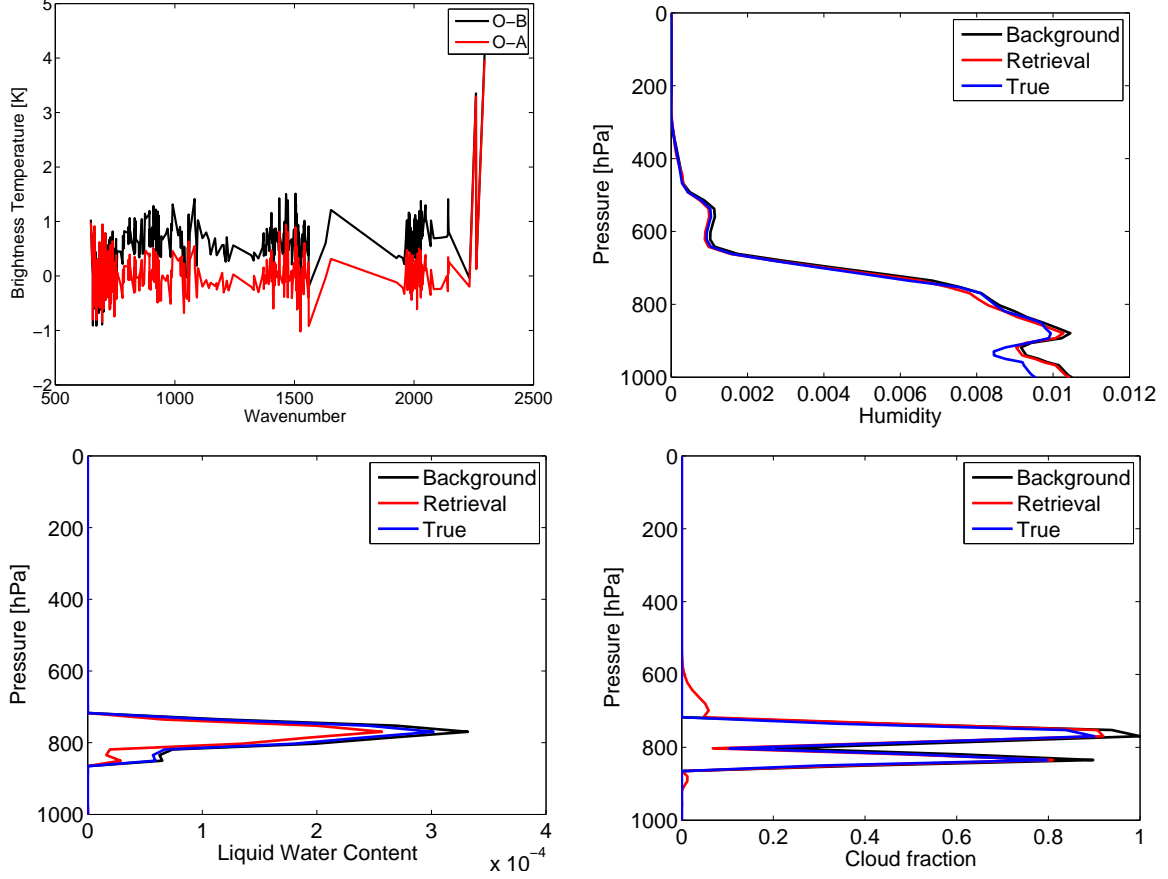


Figure 3: Low liquid cloud experiment: O-B and O-A (top left panel), humidity (top right panel), liquid water (bottom left) and cloud fraction profiles (bottom right) for the background (black line), the ‘true’ profile (blue line) and the analysis (red line).

3.2 Linear error analysis of IASI cloudy radiances

In order to understand the 1D-Var increments shown in the previous section, as well as the information content of IASI cloudy radiances, the analysis error covariance matrix \mathbf{A} of the optimal state obtained after the minimization of the cost function has been calculated. The \mathbf{A} matrix is expressed by:

$$\mathbf{A}^{-1} = \mathbf{B}^{-1} + \mathbf{H}^T \mathbf{R}^{-1} \mathbf{H} \quad (3.2)$$

where \mathbf{H} is the Jacobian matrix (partial derivatives of the brightness temperature with respect to each control variable). The Jacobians with respect to each control variable (temperature, humidity, liquid water content, ice water content and cloud fraction) for the optimal state are shown in figure 7.

For the opaque cloud, temperature and humidity Jacobians are significant above 400 hPa associated to the first ice cloud layer. The Jacobians with respect to the liquid water content are significant at atmospheric layers covered by the low liquid cloud. The sensitivity at 500 hPa is due to the creation of non negative liquid water content during the minimization by the cross-correlations between variables explained in the \mathbf{B} matrix. The Jacobians with respect to the cloud fraction are significant at levels associated to the ice cloud (200 to 400 hPa) and the liquid cloud (900 hPa).

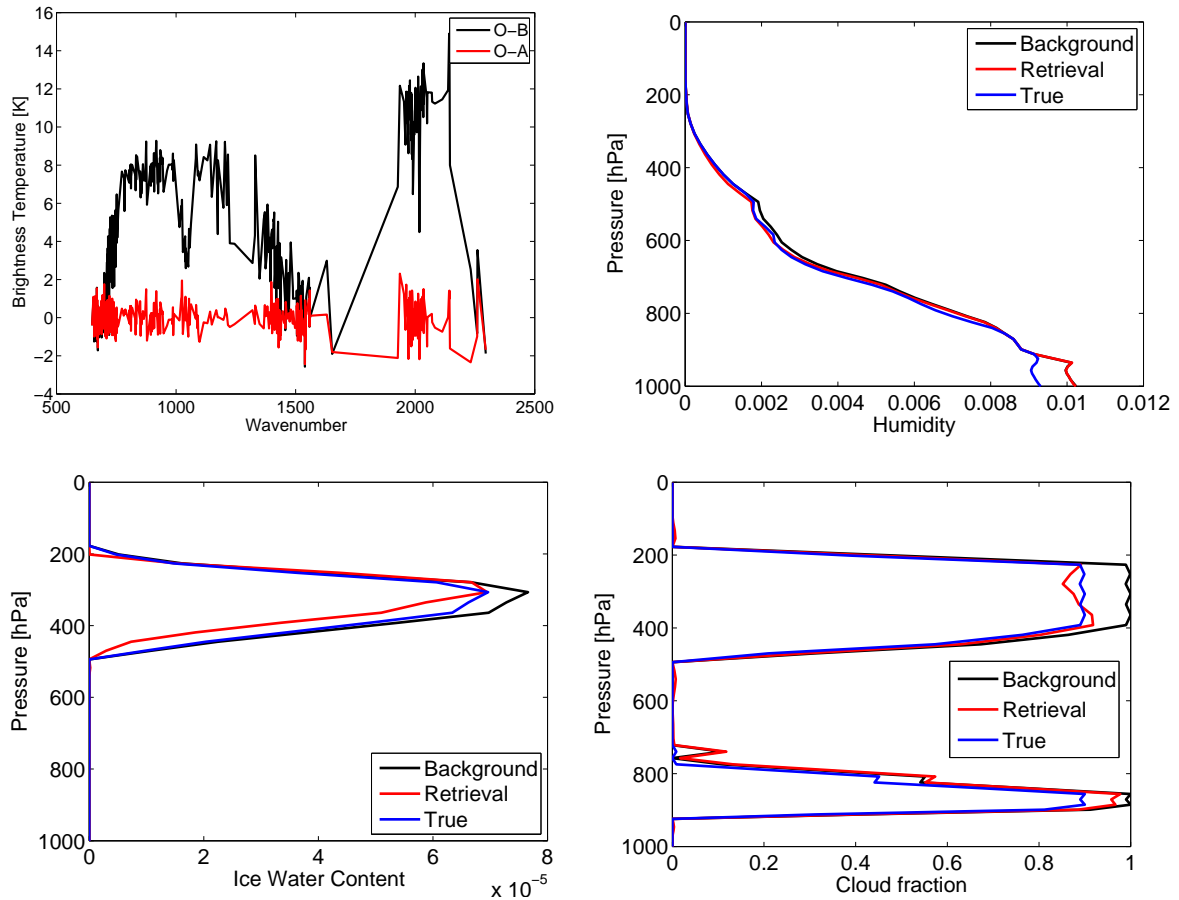


Figure 4: Opaque cloud experiment: O-B and O-A (top left panel), humidity (top right panel), ice water content (bottom left) and cloud fraction profiles (bottom right) for the background (black line), the ‘true’ profile (blue line) and the analysis (red line).

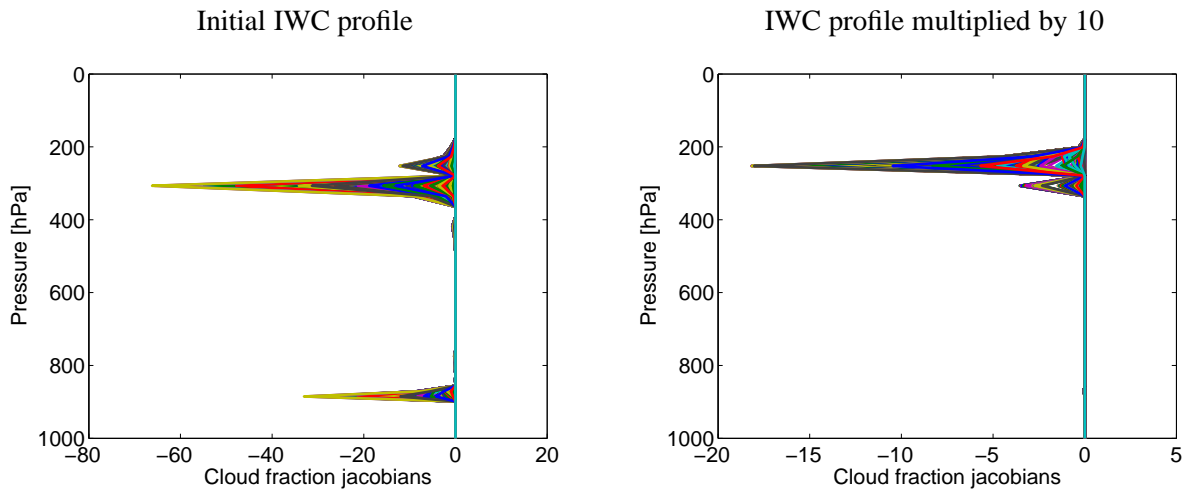


Figure 5: Opaque cloud experiment: cloud fraction Jacobians computed with the initial ice water content profile (left panel) and the initial ice water content after the multiplication by 10 (right panel).

For the semi-transparent cloud, the temperature Jacobians are significant up to 600 hPa showing a higher transparency compared to the previous cloud. The Jacobians with respect to the liquid water content are significant on the lowest atmospheric levels (under 900 hPa) due to the creation of a new liquid cloud layer by the **B** matrix cross-correlations. The Jacobians with respect to the ice water content and the cloud fraction are significant at

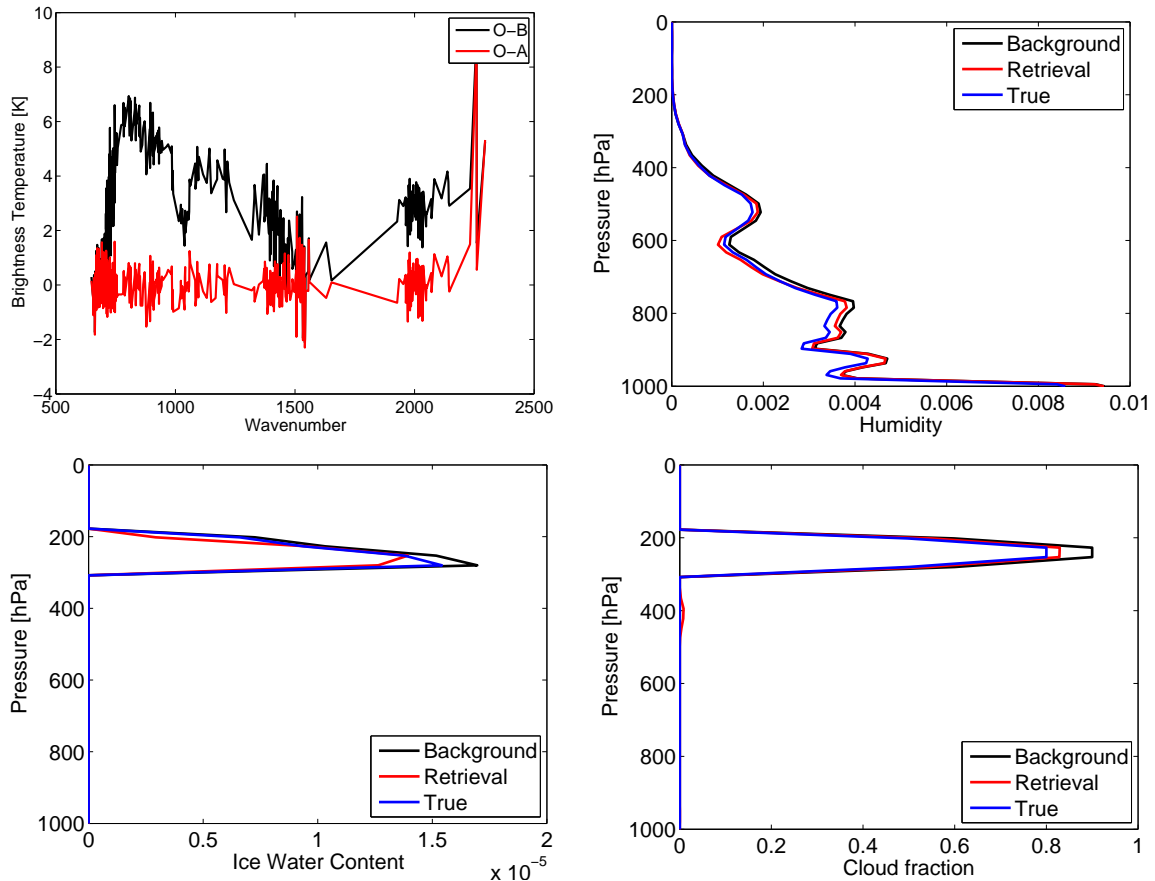


Figure 6: Semi-transparent ice cloud experiment: O-B and O-A (top left panel), humidity (top right panel), ice water content (bottom left) and cloud fraction profiles (bottom right) for the background (black line), the ‘true’ profile (blue line) and the analysis (red line).

the cloud top (250 hPa).

For the low cloud, the Jacobians with respect to the liquid water content are associated to the liquid layer between 700 and 850 hPa and to new layers that appeared at 600 hPa with the **B** matrix cross-correlations. The cloud fraction Jacobians are the most sensitive to levels just above 800 hPa associated to the cloud fraction and liquid water content maxima.

For all these cases, it is worth noting that the cloud content Jacobians are the most sensitive to the upper part of the cloud whereas the cloud fraction Jacobians peak at the level of maximum cloud fraction and cloud contents.

Figure 8 shows the cloud fraction analysis errors (diagonal elements of the **A** matrix) compared to the cloud fraction background errors (diagonal elements of the **B** matrix). Cloud fraction errors are mainly reduced at cloud levels. For the opaque cloud, the reduction is significant for both the ice cloud layer and the liquid cloud layer. For the semi-transparent cloud, the reduction is limited to the upper troposphere where the ice cloud is. For the low cloud, the main reduction is observed at 800 hPa where the cloud is with some improvement at the upper troposphere (400 hPa) due to the appearance of non-zero cloud fraction values associated to a new ice cloud layer created by the **B** matrix cross-correlations.

3.3 Conclusion

In this section, we have shown encouraging results for the inclusion of the cloud variables (liquid water content, ice water content and cloud fraction) in the control vector of the 1D-Var. The 1D-Var correctly decreases the cloud amounts to reduce the O-B departures according to the state dependent cloud Jacobians. However, we noticed some convergence problem when the cloud fraction is included in the control variables more especially

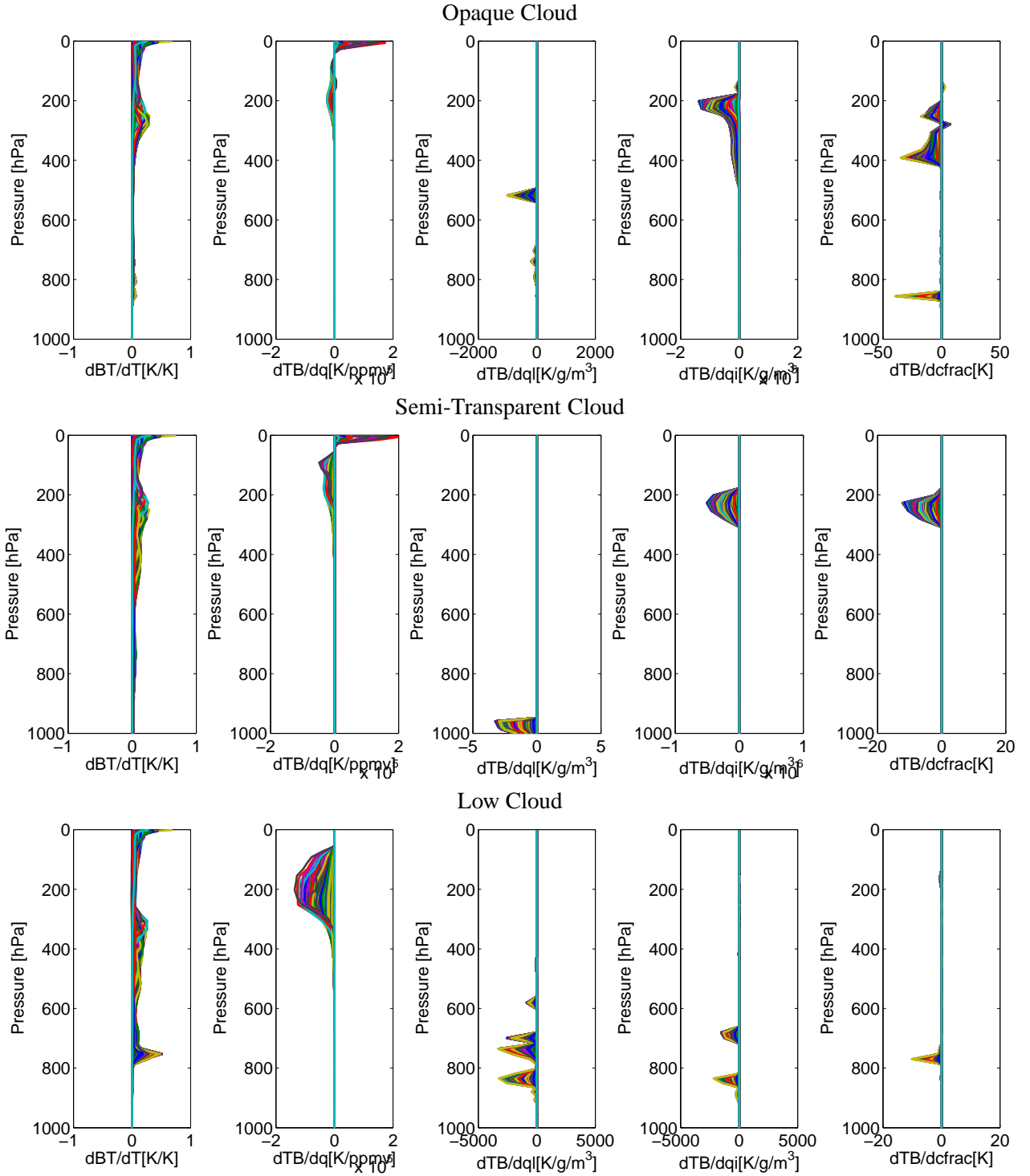


Figure 7: Jacobians with respect to each control variable from left to right: temperature, humidity, liquid water content, ice water content and cloud fraction.

for opaque clouds for which the fraction of profiles reaching convergence was decreased by 40% (only 33% instead of 72%). The 1D-Var convergence depends on three constraints :

$$abs\left(\frac{J_{cost} - J_{old}}{J_{cost}}\right) < 9.9 \times 10^{-3} \quad (3.3)$$

where J_{cost} is the new cost function calculated with the new profile and J_{old} is the old cost function.

$$\frac{\gamma}{\gamma_{old}} < 1.01 \quad (3.4)$$

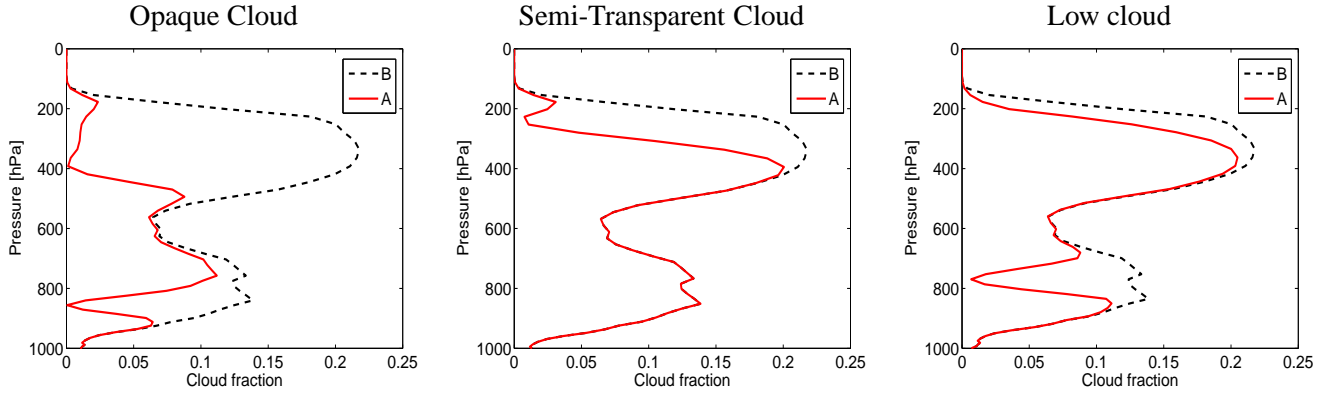


Figure 8: Cloud fraction analysis errors (red line) and background errors (dotted line) for the opaque cloud (left panel), the semi-transparent cloud (middle panel) and the low cloud (right panel).

where γ is the new gamma factor of the Levenberg-Marquardt minimization and γ_{old} the previous gamma factor.

$$\nabla J_{cost} < J_{cost}^2 \quad (3.5)$$

where ∇J_{cost} is the gradient of the cost function. To obtain a better convergence rate for opaque clouds, the constraint on the gradient of the cost function was removed to reach 84% of convergence. We did not notice a significant degradation of the analyses without this constraint. The convergence rate for low clouds is quite good even with the cloud fraction in the control variables (83% instead of 88%) and the constraint on the gradient can be kept. Semi-transparent clouds are more complicated with a convergence rate of only 38% with the cloud fraction in the control variables and 44% without. The convergence rate is increased if we relax the gradient constraint but we noticed some degradations in the analyses.

In this first section, we have treated the easiest cloudy cases where the cloudy layer is simulated in the correct vertical level by the NWP model but with an excess cloud amount. The good results obtained for these simple cases encouraged us to evaluate if it could be possible to shift the cloud in vertical levels with no cloud in the background. These cases are the most complicated as the cloud Jacobians are non zero only in layers covered by clouds.

4 Can we modify a cloud in layers that are not present in the background ?

In this section, the ‘true’ AROME profiles have been modified to shift the already existing cloud on vertical levels where there is no cloud in the background. These cases are the most complicated to treat as the cloud Jacobians are equal to zero where there is no cloud. Two example are shown where the clouds have been shifted upwards: the opaque cloud (figure 9) and the low liquid cloud (10). Surprisingly, the results are very promising. For the opaque cloud, a new ice cloud layer is created at 300 hPa with ice water content and cloud fraction profiles very close to the ‘truth’. For the low cloud, a new liquid cloud layer is also created around 750 hPa. The liquid water content and the cloud fraction are underestimated and the cloud location is slightly above the ‘true’ cloud but this second result is also very encouraging.

In order to understand how the 1D-Var is able to create new cloudy layers, we studied the 1D-Var behaviour for different \mathbf{B} matrices:

- The complete \mathbf{B} matrix with cross-correlations between variables;
- A block diagonal \mathbf{B} matrix without cross-correlations between variables;
- A block diagonal \mathbf{B} matrix without vertical correlations between adjacent levels for the cloud fraction.

The results associated to the different \mathbf{B} matrices are shown in figures 9 and 10. We can note that even without cross-correlations, the cloud is shifted upwards to fit the ‘true’ profile. However, the cloud location and cloud amount are less close to the ‘truth’ more especially in the case of the opaque cloud.

If we remove the vertical correlations between adjacent levels for the cloud fraction, the analysis does not manage to create the new cloudy layer. The cloud fraction increment is confined at the cloud top level already existing in the background. For the opaque cloud, we can also note the high humidity increment in the upper troposphere which does not seem sensible proving some deficiencies in the 1D-Var.

Figure 11 shows the cloud fraction profiles obtained during the first three iterations of the minimization in the case of the opaque cloud. We also show the cloud fraction Jacobians computed at the first iteration by the 1D-Var using the background profile. The cloud fraction Jacobians are sensitive to atmospheric levels corresponding to the maximum cloud fraction profile but also at the top of the ice cloud layer just under 400 hPa. This sensitivity just under 400 hPa is associated to a positive cloud fraction increment. If we take into account the cloud fraction vertical correlations, this increment is spread on the vertical up to 200 hPa. On the contrary, without the cloud fraction vertical correlations, the increment is confined at 400 hPa. The appearance of positive cloud fraction values between 200 and 400 hPa with the cloud fraction vertical correlations enable to create non-zero Jacobians in the upper troposphere at the second iteration to gradually shift the cloud upwards. Without the vertical correlations, the cloud fraction Jacobians above 400 hPa remain equal to zero during the minimization making impossible the creation of a new cloudy layer.

Figure 12 shows the observation minus analysis departures obtained at each iteration of the minimization for the different \mathbf{B} matrices in the case of the opaque cloud. With the complete \mathbf{B} matrix, 15 iterations are needed to make the 1D-Var converge but the O-A departures are closest to zero compared to the other experiments. In fact, with a block diagonal \mathbf{B} matrix, 9 iterations are needed for the convergence but the final O-A departures are slightly higher than 0 K, especially for window channels. With a block diagonal \mathbf{B} matrix without cloud fraction vertical correlations, 8 iterations are needed for the convergence but the final O-A departures can reach 6 K for window channels showing deficiencies during the minimization.

This study proved the important role played by the cloudy \mathbf{B} matrix during the minimization. For the analysis of cloud variables the use of state dependent \mathbf{B} matrices is still an active area of research and is very challenging for the future.

5 Root-mean-square-error (RMSE) of 1D-Var retrievals

The previous results were very promising but only few cloud cases were tested on specific background perturbations. At this stage, we decided to perform 1D-Var retrievals on a large sample of atmospheric profiles to quantify the analysis on a statistical sense. For that purpose, the background profiles are generated from the AROME profile dataset perturbed with the addition of simulated forecast errors. The forecast errors are calculated from the background error-covariance matrix \mathbf{B} such as :

$$\mathbf{x}_b = \mathbf{x}_t + \sum_i \epsilon_i \lambda_i^{1/2} \mathbf{L}_i \quad (5.1)$$

where \mathbf{x}_b is the perturbed background profile, \mathbf{x}_t is considered as the ‘true’ profile, and \mathbf{L}_i and λ_i are eigenvectors and eigenvalues of \mathbf{B} and ϵ_i is a random vector drawn from a Gaussian distribution with zero mean and unit standard deviation. From these random perturbations, cloudy layers can be either created or dissolved from the ‘true’ profile.

The observations are generated from the ‘true’ background profiles and simulated observation errors are added so that:

$$\mathbf{y} = \mathbf{H}(\mathbf{x}_t) + \epsilon_o \mathbf{R}^{\frac{1}{2}} \quad (5.2)$$

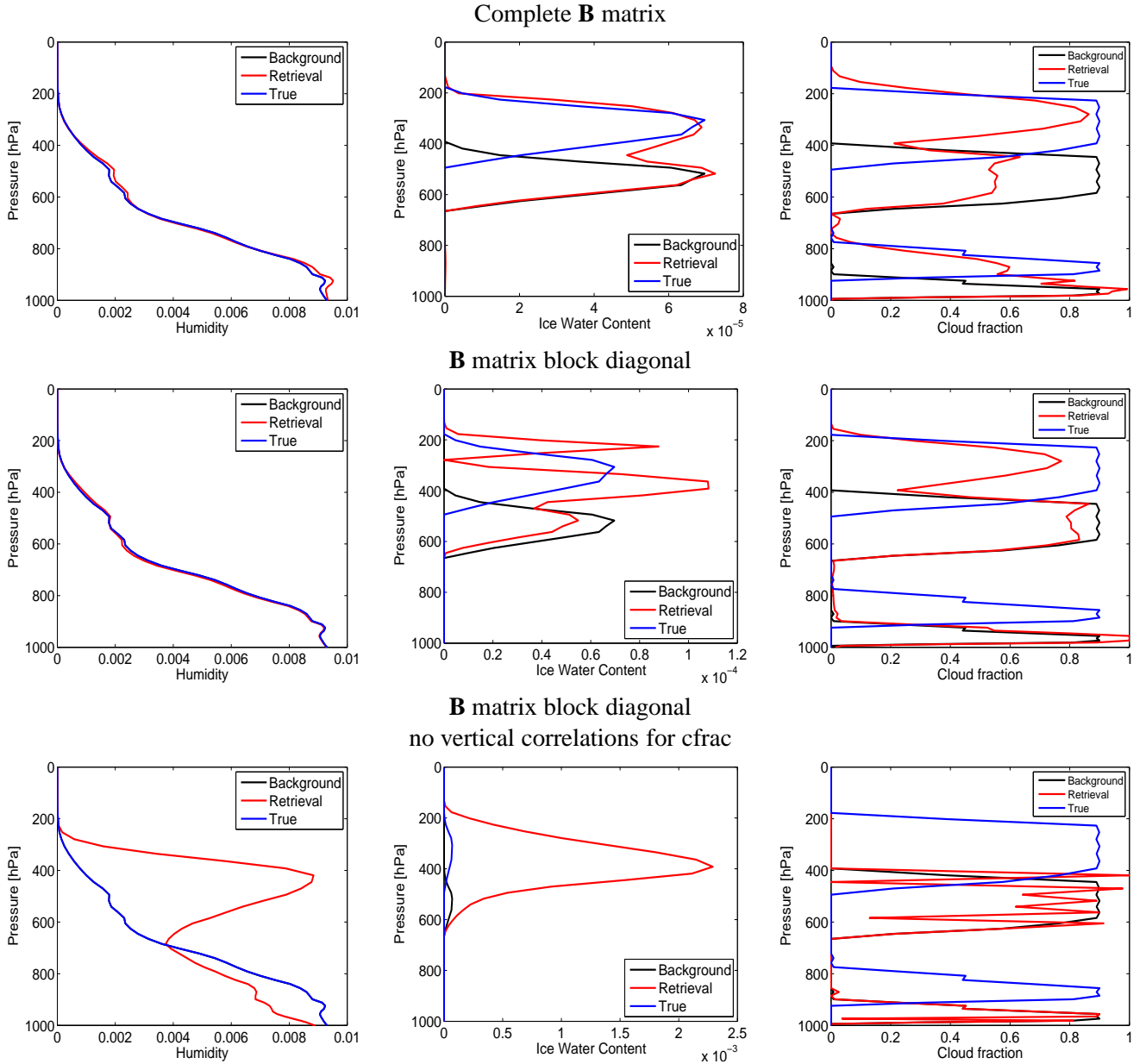


Figure 9: Opaque cloud experiment: humidity (left panel), ice water content (middle panel) and cloud fraction profiles (right panel) for the background (black line), the ‘true’ profile (blue line) and the analysis (red line).

where \mathbf{y} is the perturbed observation, $H(\mathbf{x}_t)$ is the observation simulated from the ‘true’ profile, and ϵ_o is a random vector drawn from a Gaussian distribution with zero mean and unit standard deviation.

1D-Var retrievals are performed on a subset of 588 high opaque clouds, 390 semi-transparent clouds and 240 low clouds. Mixed-phase clouds and multi-layer clouds are taken into account in the experiment. Figures 13, 14, and 15 show the root-mean-square-errors of the analysis and the background against the ‘truth’ for opaque clouds, low clouds and semi-transparent clouds respectively.

For opaque clouds, the analyses of ice water content and cloud fraction in the upper troposphere are improved compared to the background. The temperature analysis is also better than the background in the stratosphere. However, significant background degradations are observed for humidity, liquid water content and cloud fraction under 500 hPa.

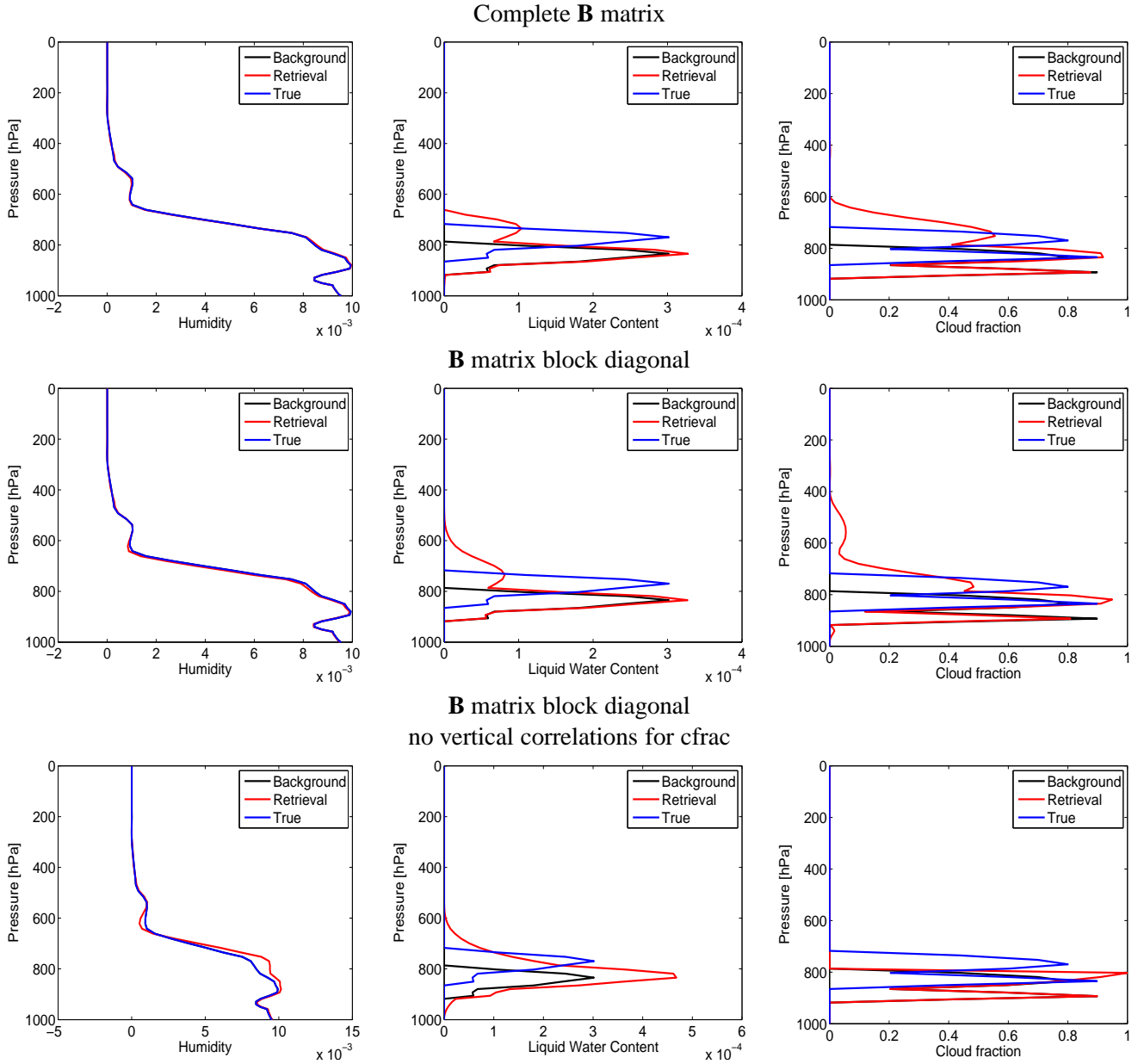


Figure 10: Low cloud experiment: humidity (left panel), liquid water content (middle panel) and cloud fraction profiles (right panel) for the background (black line), the ‘true’ profile (blue line) and the analysis (red line).

For low clouds, the improvements are more prominent with a very good contribution of the cloudy soundings to all the atmospheric column for all the variables. However, we can notice some degradations in the humidity, liquid water content and cloud fraction analyses around 900 hPa. These degradations are still very small and limited to few atmospheric levels.

For semi-transparent clouds, the analyses are better than the backgrounds for the cloud fraction, the liquid water content and the ice water content. The impact on temperature is neutral with no significant degradations or improvements. The humidity analysis is improved for the upper troposphere above 700 hPa but some small degradations are also observed at 700 hPa and 900 hPa.

The degradations observed on humidity and cloud variables for the low troposphere are probably due to non-linearities that are not taken into account in the 1D-Var. These non-linearities cannot be detected with only the study of the analysis error covariance matrix \mathbf{A} which is computed in the context of linear estimation theory.

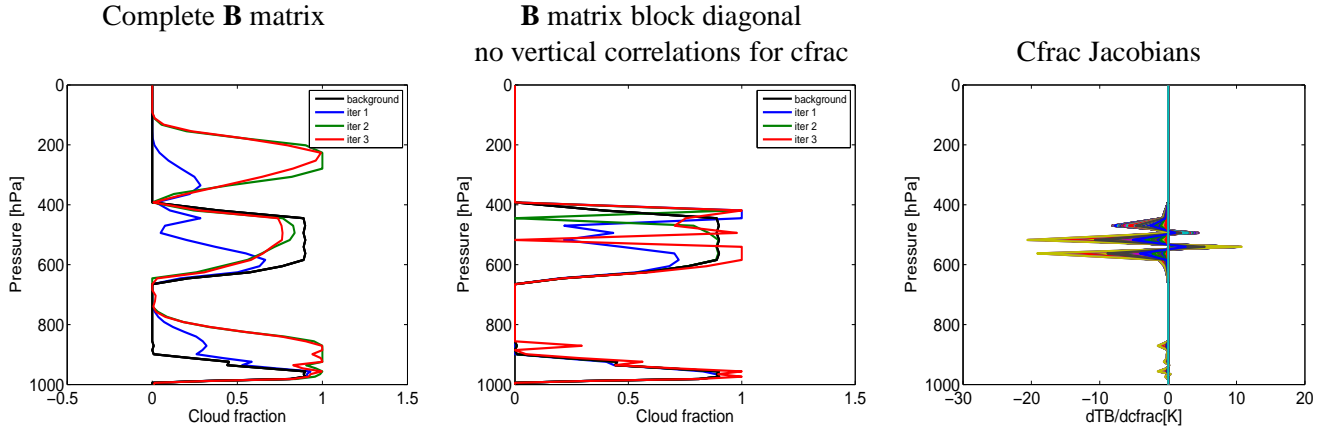


Figure 11: Opaque cloud experiment: Cloud fraction profiles obtained at the first three iterations of the 1D-Var minimization with the complete \mathbf{B} matrix (left panel) and with a block diagonal \mathbf{B} matrix with no vertical correlations for the cloud fraction (middle panel). Cloud fraction Jacobians computed at the first iteration from the background profile (right panel)

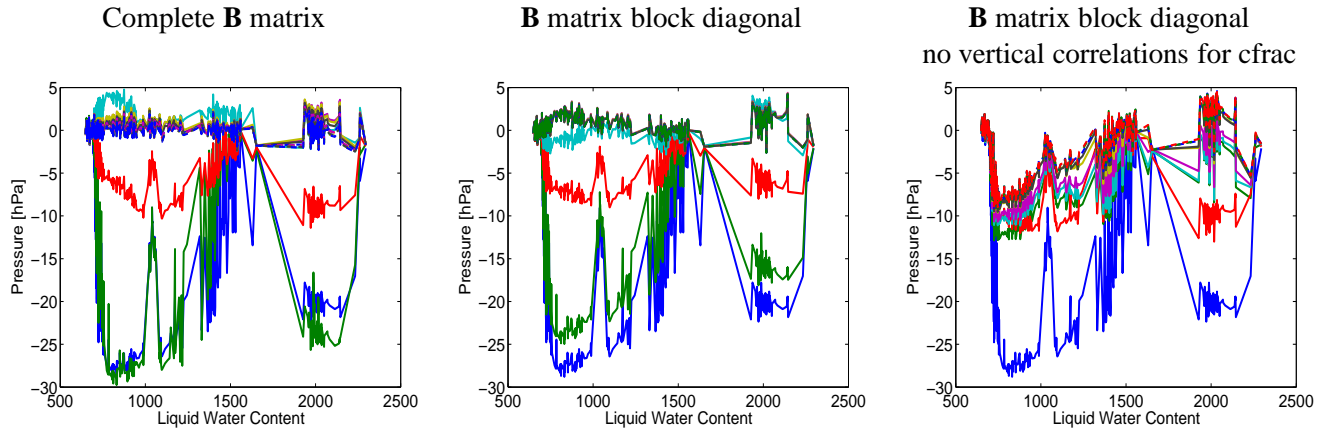


Figure 12: Opaque cloud experiment: Observation minus analysis at each iteration of the 1D-Var minimization with the complete \mathbf{B} matrix (left panel, 15 iterations), with a block diagonal \mathbf{B} matrix (middle panel, 9 iterations) with a block diagonal \mathbf{B} matrix with no vertical correlations for the cloud fraction (right panel, 8 iterations).

However, the results seem encouraging with good improvements of the cloud fraction and the cloud variables for most cloudy cases on average.

6 Conclusion

This study was a preliminary investigation for the use of the cloud fraction for the assimilation of cloud-affected IR radiances. The NWP SAF 1D-Var code was extended to include the cloud microphysical variables as new control variables: temperature, humidity, liquid water content, ice water content and cloud fraction. The convective scale model AROME was used to provide 3-h forecasts for each variable. The retrievals were validated in the context of observing system simulation experiments.

It was shown that the 1D-Var is able to increase or decrease the cloud amounts according to the observation minus background departures and the Jacobians. The 1D-Var was able to successfully modify cloudy layers already existing in the background to better fit the ‘true’ AROME profiles.

We also found promising results to shift a cloud in vertical layers not covered by clouds in the background. These cases are the most difficult but also the most interesting to deal with the cloud mislocation in NWP models. We highlighted the importance of the cloudy \mathbf{B} matrix during the 1D-Var and more especially the vertical

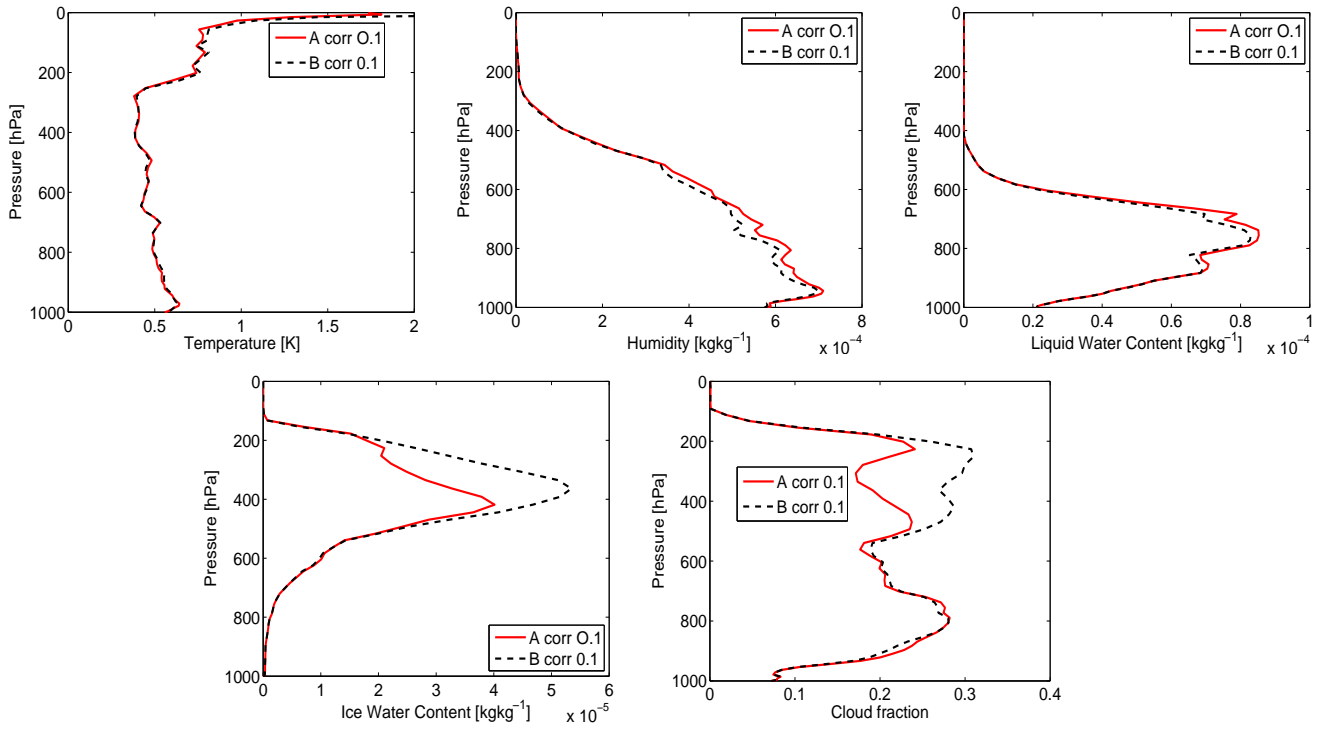


Figure 13: Opaque cloud experiment: Vertical profiles of root-mean-square errors of the background and the analysis against the ‘truth’ (dotted and plain lines respectively) for temperature (top left), humidity (top middle), liquid water content (top right), ice water content (bottom left) and cloud fraction (bottom right).

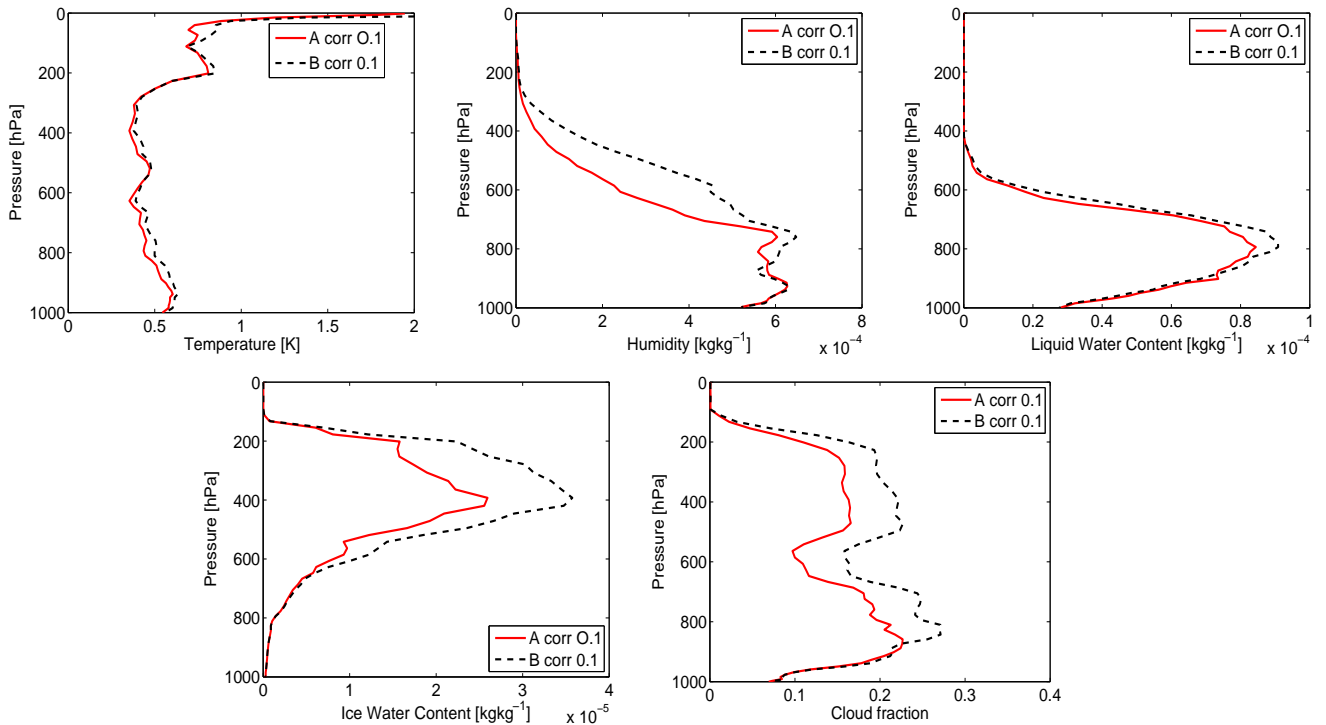


Figure 14: Low cloud experiment: Vertical profiles of root-mean-square errors of the background and the analysis against the ‘truth’ (dotted and plain lines respectively) for temperature (top left), humidity (top middle), liquid water content (top right), ice water content (bottom left) and cloud fraction (bottom right).

correlations used for the cloud fraction. In fact, without vertical correlations between adjacent levels for the

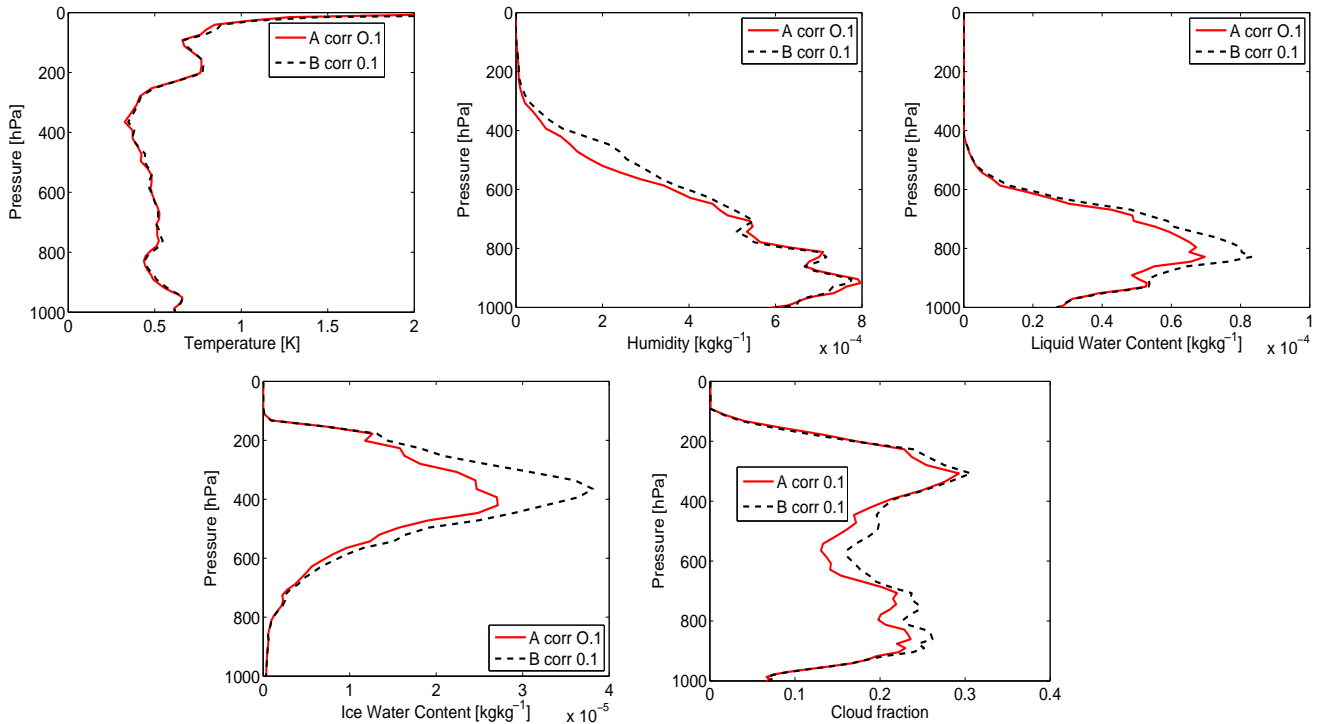


Figure 15: Semi-Transparent cloud experiment: Vertical profiles of root-mean-square errors of the background and the analysis against the ‘truth’ (dotted and plain lines respectively) for temperature (top left), humidity (top middle), liquid water content (top right), ice water content (bottom left) and cloud fraction (bottom right).

cloud fraction, the 1D-Var is not able to move the cloud in clear and dry atmospheric layers because of the non-sensitivity of cloud Jacobians at these levels. We have also shown that the reduction of the O-B departures are degraded if the cross-correlations between variables are removed from the \mathbf{B} matrix.

Finally, to generalize our results, we performed 1D-Var retrievals on a large sample of atmospheric profiles to compare the root-mean-square-errors (RMSE) of the analysis and the background against the ‘truth’. On average, the analyses are able to improve the background for all the variables. However, some slight degradations in the humidity, liquid water content and cloud fraction analyses were observed in the low troposphere probably due to non-linearities. These degradations are more significant for opaque clouds.

Even if our results are quite promising, there are many limitations and issues not covered by the study. The degradations observed in the analyses of humidity and cloud variables should be carefully investigated to understand if they come from non-linearities of cloud processes or the use of a non appropriate background error covariance matrix. The use of a cloudy \mathbf{B} matrix depending on the cloudy situation should be studied to quantify the gain in information that would be brought in the analysis of cloud variables.

Finally, an idealized framework with simulated IASI observations was used but we can hope to find similar results with real IASI observations after a careful pre-screening of data causing high non-linearities.

References

- Bauer P, Geer A.J, Lopez P, Salmond D, 2010. Direct 4D-Var assimilation of all-sky radiances. Part I: Implementation. *Quart.J.Roy.Meteor.Soc.*, **136**, 1868-1885. DOI:10.1002/qj.659
- Berre L, 2000. Estimation of synoptic and mesoscale forecast error covariances in a limited area model. *Monthly Weather Review* , **128**(3), 644-667.
- Collard A, McNally A.P, 2009. The assimilation of Infrared Atmospheric Sounding Interferometer radiances at ECMWF. *Quart.J.Roy.Meteor.Soc.*, **135**, 1044-1058.

- Desroziers G, Berre L, Pannekoucke O, Stefănescu S-E, Brousseau P, Auger L, Chapnik B, Raynaud L, 2008. Flow-dependent error covariances from variational assimilation ensembles on global and regional domains. *HIRLAM Technical Report No. 68*.
- Fourrié N, Rabier F, 2004. Cloud characteristics and channel selection for IASI radiances in meteorologically sensitive areas. *Quart.J.Roy.Meteor.Soc.*, **128**, 2551-2556.
- Geer A.J, Bauer P, Lopez P, 2008. Lessons learnt from the operational 1D+4D-Var assimilation of rain and cloud-affected SSM/I observations at ECMWF. *Quart.J.Roy.Meteor.Soc.*, **134**, 1513-1525.
- Geer A.J, Bauer P, Lopez P, 2010. Direct 4D-Var assimilation of all-sky radiances part II: Assessment. *Quart.J.Roy.Meteor.Soc.*, **136**, 1886-1905.
- Guidard V, Fourrié N, Brousseau P, Rabier F, 2010. Impact of IASI assimilation at global and convective scales and challenges for the assimilation of cloudy scenes. *Quart.J.Roy.Meteor.Soc.*, DOI: 10.1002/qj.928, **137**, 1975-1987.
- Hocking J, Rayer P, Saunders R, Matricardi M, Geer A, Brunel P, 2010. RTTOV v10 Users Guide .NWPSAF-MO-UD-023, EUMETSAT, Darmstadt, Germany.
- Lavanant L, Fourrié N, Gambacorta A, Grieco G, Heillette S, Hilton F, Kim M-J, McNally A.P, Nishihata H, Pavelin E.G and Rabier F, 2011. Comparison of cloud products within IASI footprints for the assimilation of cloudy radiances. *Quart.J.Roy.Meteor.Soc.*, **137**, 1988-2003.
- Martinet P, Fourrié N, Guidard V, Rabier F, Montmerle T and Brunel P, 2013, a. Towards the use of microphysical variables for the assimilation of cloud-affected infrared radiances. *Quart.J.Roy.Meteor.Soc.*, in press, DOI:10.1002/qj.2046.
- Martinet P, Lavanant L, Fourrié N, Rabier F, Gambacorta A, 2013, b. Evaluation of a revised IASI channel selection for cloudy retrievals with a focus on the Mediterranean basin. *Quart.J.Roy.Meteor.Soc.*, submitted.
- McNally A.P, 2009. The direct assimilation of cloud-affected satellite infrared radiances in the ECMWF 4D-Var. *Quart.J.Roy.Meteor.Soc.*, **135**, 1214-1229.
- McNally A.P, 2002. A note on the occurrence of cloud in meteorologically sensitive areas and the implications for advanced infrared sounders. *Quart.J.Roy.Meteor.Soc.*, **128**, 2551-2556.
- Michel Y, Auligné T, Montmerle T, 2011. Heterogeneous Convective-Scale Background Error Covariances with the Inclusion of Hydrometeor Variables. *Monthly Weather Review*, **139**, 2994-3015.
- Montmerle T, Berre L, 2010. Diagnosis and formulation of heterogeneous background-error covariances at the mesoscale. *Quart.J.Roy.Meteor.Soc.*, **136**, 1408-1420.
- Pangaud T, Fourrié N, Guidard V, Dahoui M, Rabier F, 2009. Assimilation of AIRS Radiances affected by Mid-to Low-Level Clouds. *Monthly Weather Review*, **137**, 4276-4292.
- Pavelin E.G, English S.J, Eyre J.R, 2008. The assimilation of cloud-affected infrared satellite radiances for numerical weather prediction. *Quart.J.Roy.Meteor.Soc.*, **134**, 737-749.
- Pavelin E.G, Collard A, 2009. NWP SAF Met Office 1D-Var User Manual. *NWPSAF-MO-UD-006*.